

Manuscript Number:

Title: RF Strip-Line Anodes for Psec Large-Area MCP-based Photodetectors

Article Type: Research Paper

Section/Category: Gamma, X-ray and Charged Particle Detectors

Keywords: photodetector, anode, microstrip, stripline, microchannel plate, analog bandwidth, large-area detector

Corresponding Author: Prof. Henry Jonathan Frisch, Ph.D,

Corresponding Author's Institution: University of Chicago

First Author: Herve Grabas

Order of Authors: Herve Grabas; Henry Jonathan Frisch, Ph.D.; Eric Oberla; Jean-Francois Genat; Richard Northrop; David McGinnis; Bernhard Adams; Matthew Wetstein, Ph.D; Razib Obaid

Abstract: We have designed and tested economical large-area RF strip-line anodes made by silk-screening silver onto inexpensive plate glass, for use in microchannel plate photodetectors to provide measurements of time, position, integrated charge, and pulse waveform shapes. The 229-mm-long anodes are modular, and can be attached in series for economy in electronics channel-count. Measurements of the anode impedance, bandwidth and cross-talk due to inter-strip coupling are presented. The analog bandwidth, a key determinant of timing resolution, decreases from 1.6 GHz to 0.4 GHz as the anode length increases from 289 mm to 916 mm.

THE UNIVERSITY OF CHICAGO
THE ENRICO FERMI INSTITUTE

5640 SOUTH ELLIS AVENUE

CHICAGO · ILLINOIS 60637-1433

phone: (773) 702-7479 / fax: (773) 702-1914

August 28, 2012

Dr. W. Barletta
Coordinating Editor
Nuclear Instruments and Methods in Physics Research Section A
Massachusetts Institute of Technology
Cambridge, MA, USA

Dear Dr. Barletta:

This is the cover letter with the items requested by Elsevier for the manuscript “RF Strip-Line Anodes for Psec Large-Area MCP-based Photodetectors”. We greatly appreciate your time and effort and thank you in advance.

To our knowledge we do not require any special considerations.

A brief background is as follows. In 2009 we proposed to the DOE a project (now the LAPPD Collaboration [1]) to develop very fast (several picosecond-resolution) large-area photodetectors for use in TOF systems at colliders and, at lower resolution (100 psec), for large-area coverage in underground detection of neutrinos, using Cherenkov light. To cover large-areas inexpensively while preserving the time resolution method of digitizing the signal we proposed RF-quality transmission line anodes with bandwidths matched to the fast signals inherent in a small-pore microchannel plate (MCP) [2]. We are now at the 3-year anniversary of the R&D funding, and are in the process of documenting the essential aspects of the detector development and performance.

The use of MCP's as TOF detectors with the small intrinsic spatial scale (typically pores are 10-20 microns in diameter) necessary for small fluctuations in timing due to path length variations, but scalable to large areas grew out of a talk on the future.- of high energy physics at the Aspen Winter conference in 2003 [3]. The understanding of the determinants of timing resolution has grown through a series of workshops [4]. Briefly, the resolution is predicted to depend inversely on the signal-to-noise ratio, and inversely on the risetime of the pulse for a constant number of measurements on the leading edge of the pulse [5, 6]. Early work by others includes a seminal paper by Ohshima and the Nagoya group [7].

Two of the enabling technologies for the LAPPD detectors are waveform sampling front-end electronics [8], and an anode that collects the charge from the MCP and retains the analog bandwidth of the MCP pulse. The paper we

are submitting describes designing and testing the anode we have chosen for the LAPPD detectors.

The Corresponding Author is:

Prof. Henry Frisch
HEP320, EFI
5640 S. Ellis Ave
Chicago IL
frisch@hep.uchicago.edu

Reference [5] describes a previous submission on the simulation studies that led to the anode design.

Sincerely,

Henry Frisch
Professor of Physics
Enrico Fermi Institute and Physics Department

References

- [1] The original LAPPD institutions include ANL, Arradiance Inc., the Univ. of Chicago, Fermilab, the Univ. of Hawaii, Muons, Inc, SLAC, SSL/UCB, and Synkera Corporation. More detail can be found at <http://psec.uchicago.edu/>.
- [2] T. Credo, H. Frisch, H. Sanders, R. Schroll, and F. Tang; Proceedings of the IEEE, Rome, Italy, Oct. 2004; Nuclear Science Symposium Conference Record, 2004 IEEE, Volume 1
- [3] H. Frisch, *Visions of Experimental Particle Physics— Where Are We Going?*, Aspen Winter Conference, Aspen Co., Jan. 26, 2003 (<http://hep.uchicago.edu:frisch>)
- [4] For a list of the workshops and links to the talks, see <http://psec.uchicago.edu/workshops>.
- [5] J.-F. Genat, G. Varner, F. Tang, H. Frisch; *Signal Processing for Pico-second Resolution Timing Measurements*; Nucl.Instrum.Meth.A607:387-393, Oct., 2009. e-Print: arXiv:0810.5590
- [6] S. Ritt, in *The Factors that Limit Time Resolution in Photodetectors*; Workshop, Univ. of Chicago, Chicago, IL; 28-29 April 2011. See <http://psec.uchicago.edu/workshops/> Note that of the values needed of the four parameters to achieve a time resolution of 100 fsec (the bottom row of the table of extrapolations), we have achieved or exceeded three: sampling rate, noise, and signal size. Only the analog bandwidth falls short at present.

- [7] K. Inami, N. Kishimoto, Y. Enari, M. Nagamine, and T. Ohshima; Nucl. Instrum. Meth. A560, 303-308, 2006
- [8] E. Oberla, *A Fast Waveform-Digitizing ASIC-based DAQ for a Position & Time Sensing Large-Area Photo-Detector System*; Photodet2012, LAL Orsay, France; June, 2012

1 RF Strip-Line Anodes for Psec Large-Area MCP-based
2 Photodetectors

3 Hervé Grabas^a, Razib Obaid^a, Eric Oberla^a, Henry Frisch^a, Jean-Francois
4 Genat^{a,1}, Richard Northrop^a, David McGinnis^b, Bernhard Adams^c, Matthew
5 Wetstein^{c,2}

6 ^a*Enrico Fermi Institute, University of Chicago*

7 ^b*European Spallation Source, Lund, Sweden*

8 ^c*Argonne National Laboratory*

9 **Abstract**

We have designed and tested economical large-area RF strip-line anodes made by silk-screening silver onto inexpensive plate glass, for use in microchannel plate photodetectors to provide measurements of time, position, integrated charge, and pulse waveform shapes. The 229-mm-long anodes are modular, and can be attached in series for economy in electronics channel-count. Measurements of the anode impedance, bandwidth and cross-talk due to inter-strip coupling are presented. The analog bandwidth, a key determinant of timing resolution, decreases from 1.6 GHz to 0.4 GHz as the anode length increases from 289 mm to 916 mm.

¹Present address, LPNHE, CNRS/IN2P3, Universités Pierre et Marie Curie and Denis Diderot, T33 RC, 4 Place Jussieu 75252 Paris CEDEX 05, France

²Joint Appointment with the Enrico Fermi Institute, University of Chicago

10 **1. Introduction**

11 The development of large-area (m^2) photodetectors with time resolutions
12 of picoseconds (10^{-12} sec) and sub-millimeter space resolutions would open
13 new opportunities in many areas, including collider detectors, rare kaon ex-
14 periments, and neutrino experiments in particle and nuclear physics, X-ray
15 detection at light sources, and Time-of-Flight Positron Emission Tomography
16 (TOF-PET) [1, 2]. Micro-Channel Plate Photomultipliers (MCP-PMTs) [3]
17 have previously been shown to provide space resolutions of a few microns [4],
18 time resolutions down to 5 psec [5], and very fast risetimes [6]. MCP-based
19 detectors with bandwidths in the GHz regime are predicted to give sub-psec
20 time resolutions [2, 7].

21 Capacitively-coupled anodes have been developed with good space and time
22 resolutions for a number of applications [8–11]. In this paper we describe the
23 design and testing of economical strip-line anodes with RF analog bandwidths
24 in the GHz range and lengths up to 80 cm being developed by the LAPPD Col-
25 laboration [12] for large-area MCP-based photodetectors. The proof-of-concept
26 design described here was set at a point in the parameter space of cost, time
27 resolution, space resolution, area covered per channel, and channel density, ap-
28 propriate for applications requiring large area, low cost, and modest resolutions
29 (<10 psec in time and 400 microns in space for signals from charged particles
30 and high-energy photons, and <100 psec and 2 mm for single visible photons).
31 A different optimization of the design would allow the construction of higher
32 performance anodes for applications that require better resolution [13].

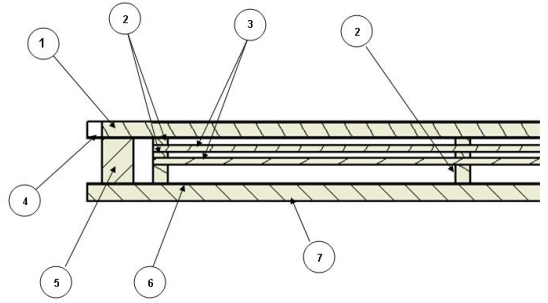
33 The LAPPD design is based on an MCP consisting of a 20-cm-square capil-
34 lary glass plate with 20- μm pores [14], functionalized with resistive and emissive
35 layers using Atomic Layer Deposition [15–18]. This method allows separately
36 optimizing the three functions performed by a conventionally constructed MCP:
37 providing the pore structure, a resistive layer for current supply, and the sec-
38 ondary emitting layer. In addition, the Incom substrates are a hard glass,
39 providing a more chemically stable platform and improved mechanical strength.

40 The structure of the LAPPD MCP-PMT vacuum photodetector is shown
41 in Figure 1 [12]. A photo-cathode is deposited on the vacuum side of the top
42 window, which is followed by an accelerating gap for the initial photo-electron,
43 a pair of 20-cm²-square MCPs in a chevron geometry that amplify the single
44 electron by a factors up to 5×10^7 , a gap after the output of the second MCP, and
45 an anode plane that collects the amplified pulse of electrons. Incident photons
46 are converted into electrons by the photo-cathode. Each of these photo-electrons
47 is accelerated into a pore of the micro-channel plate where it causes a cascade
48 by the process of secondary emission. The electrons emerging from the far ends
49 of the pores are then accelerated towards an anode where they are collected.
50 Measuring the time and position of the anode pulse gives both time and space
51 resolution information on the incoming particle [8–11]. The intrinsic granularity
52 is set by the pores; there are approximately 80 million pores in one of the 8”
53 20-micron pore Incom glass substrates in the baseline LAPPD design [14]. The
54 granularity of the readout is set by the anode pattern, which is quite flexible,
55 allowing many possible patterns and channel sizes [19]. The current 8” Incom
56 plates have open-area ratio of approximately 65% [14].

57 *1.1. Picosecond timing measurement and spatial resolution*

58 The 20-micron scale of the MCP pores sets the intrinsic time scale of the
59 pulse formation. Risetimes down to 60 psec have been measured with microchannel-
60 plate detectors [6]. The time resolution is set by the size of the pore, with smaller
61 pores producing faster rise times and smaller transit-time spreads [6]. MCP’s
62 are spatially homogeneous, and so an essential step in developing fast systems
63 with areas measured in meters-squared is the development of a large-area inex-
64 pensive anode with an analog bandwidth capable of retaining the intrinsic speed
65 of the pulse. Extrapolations to higher bandwidth predict time resolutions down
66 to 100 fsec [7].

67 The potential exists for even faster MCP risetimes by using smaller pore
68 sizes supported by the stronger glass of the substrate, higher secondary emission
69 yield (SEY) materials at the top of the pores, and ALD-based discrete dynode



- | | |
|---|-----------------------------|
| 1. Top window with photocathode on inside | 5. Side wall |
| 2. Grid spacers | 6. Anode transmission lines |
| 3. Microchannel plates | 7. Bottom window |
| 4. HV contact | |

Figure 1: The basic structure of the glass LAPPD MCP-PMT detector. The sealed vacuum tube consists of a top window with the photocathode on the inner surface, an accelerating gap for the initial photo-electron, a pair of 20-cm-square MCPs in a chevron geometry that amplify the photo-electron by factors up to 5×10^7 , a gap after the output of the second MCP, and the anode that collects the exiting ‘cloud’ of electrons. The package is less than 15 mm thick.

70 structures inside the pores [20].

71 Spatial resolution also depends on the small feature size of the MCP pores,
 72 which provide an intrinsic resolution on the order of the size of the pore. Mea-
 73 surements with spatial resolutions down to 2 microns have been reported using
 74 strip-line anodes [4]. The present anode design could be optimized for smaller-
 75 area (up to 10’s of m^2) applications requiring better resolution by the use of
 76 higher-bandwidth, higher-cost materials, and different choices of the strip-line
 77 geometric parameters, at the cost of larger channel counts.

78 1.2. Outline

79 A brief outline of the paper as a guide to the reader follows. The calcula-
 80 tion of time and position using the time-of-arrival of the pulses at both ends of
 81 the strips of the transmission line anode is presented in Section 2. Section 3 de-
 82 scribes the anode construction of inexpensive plate glass and silk-screened silver

83 strips. Measurements of the time-domain response in 20-cm and 60 cm 30-strip
84 anodes and a 20-cm 40-strip anode are presented in Section 4.3. The techniques
85 and test setups used to make the measurements of bandwidth, impedance, at-
86 tenuation, and cross-talk in the frequency domain are described in Section 4.
87 Sections 5, 6, and 7 present measurements and predictions of anode impedance;
88 bandwidth; and attenuation and crosstalk, respectively. Section 8 summarizes
89 the conclusions. Appendix A compares measurements and predictions for the
90 bandwidth and impedance of a single isolated strip.

91 **2. Using RF Strip-line anodes and wave-form sampling to measure** 92 **position, time, and properties of the pulses**

93 The charge cloud of the electrons emerging from the pores of the MCP stack
94 holds both the space and time information generated by the initial photon or
95 relativistic charged particle impinging on and traversing the window [21]. In
96 the LAPPD design, shown in Figure 1, the charge cloud propagates towards
97 an array of multiple striplines. On each stripline, the pulses created by the
98 charge excitation propagate in opposite directions to the ends of the line, where
99 they are digitized by waveform sampling. From the digitized pulses at each
100 end one can determine the time, position, total charge, and pulse shape of the
101 impinging particles. The spatial location of the charge along the strip direction
102 is determined from the difference in times measured on the two ends of a strip.
103 The one-dimensional nature preserves the excellent space resolution but with
104 many fewer channels than with a two-dimensional pixel array. In the transverse
105 direction the resolution is determined by the strip spacing in the present 1-
106 dimensional implementation of the anode [22]. The time of the deposited charge
107 is given by the average of the times at the two ends of the strip.

108 The precision of both time and space measurements depends on four param-
109 eters of the pulses that arrive at the end of a strip [2, 7]: 1) the signal-to-noise
110 ratio; 2) the risetime of the pulse; 3) the sampling frequency of the digitization;
111 and 4) fluctuations in the signal itself. The risetime of the pulse will be limited

112 by the analog bandwidth of the strip-line for applications with low-cost large-
 113 area readout [2, 19]. It is the analog bandwidth of the strip-lines that is the
 114 focus of this paper.

115 Figure 2 shows the equivalent electrical circuit of the anode. The strip-lines
 116 are formed by silk-screened silver strips on the top layer of the glass plate that
 117 forms the bottom of the vacuum volume. The sealed planar vacuum tube (See
 118 Figure 1) sits on a copper sheet, which acts as the ground plane for the strip-line.
 119 Each strip-line is terminated in 50Ω s at each end.

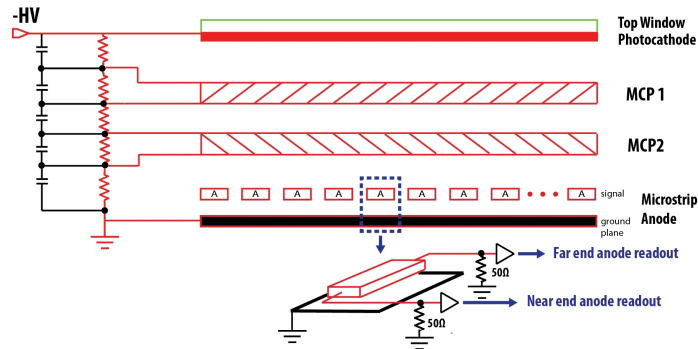


Figure 2: The equivalent electrical circuit of the strip-line anode. The strip-lines are formed by silk-screened silver strips on the top layer of the glass plate that forms the bottom of the vacuum volume. The sealed planar vacuum tube (See Figure 1) sits on a copper sheet, which acts as the ground plane for the strip-line. Each strip-line is terminated in 50Ω s at each end.

120 The time-of-arrival information at each end of a strip is extracted from the
 121 leading edge, the peak, and a portion of the trailing edge of the pulse just
 122 beyond the peak, at each end of the strip [2]. The measurement of relative
 123 times-of-arrival at the two ends benefit from the inherent correlation between
 124 the shapes of the pulses at each end of the strip. Using a commercial MCP
 125 excited by a laser as a source, we have measured a relative resolution of 2 psec
 126 on a 5"-ceramic-substrate strip-line anode [23]. Using a pair of the LAPPD 8"
 127 MCPs [24] we have measured a relative resolution of <5 psec on the 9"-long
 128 low-cost glass substrate of the LAPPD anode [24].

129 The difference in times-of-arrival between the pulses recorded at the two
130 ends of the strips provides a measurement of the position of the incident radi-
131 ation in the direction along the strips. The anodes used here have a nominal
132 impedance of 50Ω and a measured propagation velocity of $0.57\pm 0.07 c$ ($170\pm$
133 21 microns/psec). The correspondence between the position resolution (δx) and
134 the time resolution of the pulse (δt) is given by $\delta x \approx 1/2 \delta t$.

135 The position in the direction transverse to the strips is measured by digi-
136 tizing the signals on all the strips in the single-layer (i.e. 1-dimensional) anode
137 design presented here. The strip or strips closest to the position of the inci-
138 dent radiation will carry the largest signal. The neighboring strips carry signals
139 induced capacitively and inductively (see Section 7). While energy is trans-
140 ferred from the central strip into the neighboring strips, not all information is
141 lost, as the neighboring strips are digitized. In the ideal limit of zero noise the
142 information can be completely recovered in the case of a single hit.

143 A benefit of the wave-form digitization readout is that it gives the equivalent
144 of an oscilloscope trace for both ends of each of the striplines, allowing the ex-
145 traction of amplitude, integrated charge, shape, and separation of overlapping
146 or near-by pulses ('pile-up') [2]. The measured shape will depend on the ana-
147 log bandwidth, cross-talk, attenuation, and signal-to-noise of the system, and
148 will thus depend on the position of the incident excitation for large systems.
149 In addition, care has to be taken in impedance matching the detector to the
150 electronics to avoid losses from reflections at interfaces.

151 Reference [2] contains a comparison of methods to extract the time-of-arrival
152 of a pulse. A study of the benefit of using a more sophisticated fit to the pulse
153 shape is presented in Ref. [25]. Waveform sampling allows extracting much
154 more information than just the time, however; a fit to a template shape allows
155 the extraction of the amplitude, integrated charge, a figure-of-merit for the
156 goodness of fit to the shape, and possible separation of nearby or overlapping
157 pulses. Algorithms such as these can be implemented in FPGA-based processors
158 located close to the waveform digitization front-end, allowing only the higher-
159 level parameters of the pulse to be transmitted to the next level of analysis.

160 **3. Anode Design and Construction**

161 The aim of the LAPPD project is to develop a large-area economical pho-
162 todetector with good space and time resolution, low electronics channel count
163 and power, and low noise. We have developed a mechanical design based on
164 inexpensive commercial float (plate) glass [26]. This glass can be water-jet cut,
165 and so many aspects of the construction are widely available and standard in
166 industry. In this section we describe the application of these principles to the
167 design and construction of the anode.

168 *3.1. Choice in Anode Parameter Space for the Proof-of-Concept Detector*

169 The LAPPD project was started in 2009 with the goal of developing a com-
170 mercializable module in three years. Choices had to be made for the initial pa-
171 rameters for proof-of-concept, with the understanding that after the three-year
172 R&D phase, modules for specific applications would be designed with optimized
173 parameters. The parameters of the initial design described here were chosen to
174 be appropriate for applications requiring large area, low cost, and modest res-
175 olutions. The flexibility of the design, however, should allow optimizations for
176 very precise timing at colliders and other applications.

177 The initial choice of an 8"-square (200 mm) module was made to be signifi-
178 cantly larger than available MCP-PMT's but sized to widely-available vacuum
179 components and light enough to be handled by vacuum transfer equipment. In
180 addition, a 200-mm anode is long enough to be treated as a transmission line
181 for typical MCP risetimes.

182 The glass package as well as the anode glass substrate were chosen for cost
183 considerations - borofloat glass [26] is widely available and inexpensive. Evap-
184 oration and sputtering to form the metallized striplines on the surface of the
185 anode were successfully tried; however the silk-screening of silver-loaded ink [27]
186 proved significantly less expensive with a very fast turnaround, as a silk-screen
187 is much more easily produced than a mask, and the silk-screening process is
188 entirely mechanized and in air rather than in vacuum. The high-frequency be-

189 havior of the glass and silk-screened silver are adequate to handle the bandwidth
190 of the present generation of 20-micron pore MCP's.

191 The choice of the anode strip width was set by a choice of a 50Ω strip
192 impedance. This is determined by the thickness of the glass anode substrate
193 (2.75 mm) and the dielectric constant of the glass [26] (see Appendix A).

194 The choice of the gap spacing between the anode strips depends on com-
195 peting considerations. The crosstalk between strips decreases with gap size.
196 However a large gap provides an area on which charge can accumulate, leading
197 to hysteresis and possible breakdown at high rates. A larger gap size diminishes
198 the electronics channel count but increases the transverse spatial resolution [22].

199 *3.2. The Single Tile Anode*

200 The LAPPD design is modular, with the unit module being a sealed planar
201 vacuum volume with an 8" (200 mm)-square active area, called a 'tile'. The
202 metal strips that form the anode for the tile are formed by the inexpensive
203 technique of silk-screening a silver-based ink [27] onto the glass plate, and then
204 firing the plate at high temperature [28] to burn off the volatiles, leaving behind
205 the silver traces. The thickness of the silver trace is typically 10-15 μm . The
206 dimensions of the glass plate, 229.1 mm by 220.0 mm, are set by the design of
207 the 8"-square MCP-PMT active area. A single tile, connected to the 'fanout'
208 cards used for testing (see Section 4.1), is shown in Figure 3.

209 The impedance of the strip lines is determined by the width of the trace, the
210 thickness of the glass substrate separating the strips and the underlying copper
211 ground plane, and the dielectric coefficient [26]. More detail of the functional
212 dependencies is given in Appendix A.

213 Two anode strip patterns have been tested, one with 30 strips and the other
214 with 40, both with a 50Ω target impedance. The 40-strip anode was an initial
215 design, with small gaps between the strips to minimize static electric charging of
216 the inter-strip glass, and was well-matched to then-current waveform sampling
217 PSEC-3 ASIC which had 4 channels, requiring 10 chips per end [29]. The 30-
218 strip anode is matched to a new 6-channel ASIC [30], halving the chip count to

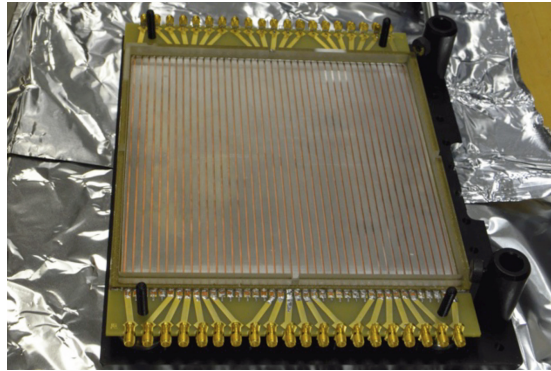


Figure 3: A single tile with a 229.1 mm-long 40-strip anode. The anode strips are connected at both ends to the fanout cards used for testing (Section 4.1).

219 5 per end. The strip width, strip gap, and plate thickness of the 30-strip anode
 220 are 4.62 mm , 2.29 mm, and 2.75 mm, respectively. The corresponding numbers
 221 for the 40-strip anode are 3.76 mm , 1.32 mm, and 2.67 mm.

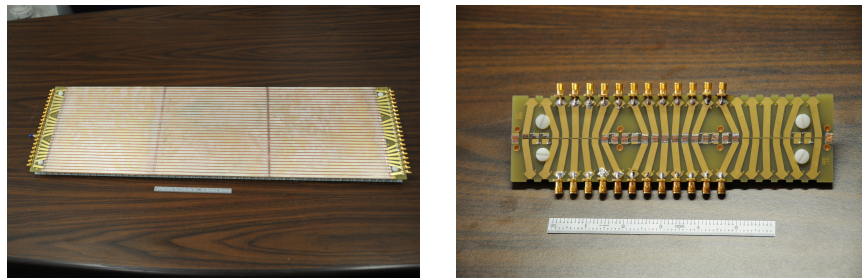


Figure 4: Left: The 3-tile anode used to measure bandwidth, attenuation, and impedance as a function of anode strip length. The connections between anode strips on neighboring tiles are made by soldering small strips of copper to the silver silk-screened strips on the glass. Right: To measure the effect of the connecting fanout cards on the bandwidth, a ‘zero tile’ consisting of just the fanout cards was constructed.

222 *3.3. The Multi-Tile Anode*

223 The strip lines of one tile can be connected in series with the strip lines of a
224 neighboring tile to make a ‘tile-row’ that shares the common readout on the two
225 ends of the shared strip, as shown in the left-hand panel of Figure 4. The strips
226 on the connected tiles form a 50Ω transmission line with the ground plane that
227 underlies all the tiles. The strips are terminated in 50Ω s at the outboard ends
228 of the first and last tile in the tile-row.

229 **4. Measurements of Anode Performance**

230 In parallel with measurements on the operational photodetector tile loaded
231 with MCP’s [24], we have made stand-alone anode measurements as described
232 below.

233 *4.1. Fanout cards*

234 To characterize the bandwidth, attenuation, and impedance of the anodes,
235 signals are introduced onto one strip from one end, and measurements are made
236 at the far and near ends of that strip and neighbors. We have made a transition
237 card that allows connections to a network analyzer, oscilloscope and/or pulse
238 generator via SMA cables, called the ‘fanout card’. Figure 3 shows a single
239 tile anode connected to transition cards on each end. The right-hand panel of
240 Figure 4 shows two fanout cards connected with no tile in-between (the ‘zero-
241 tile’); this configuration is used to measure the effect of the fanout cards on the
242 bandwidth measurements. The length of the central stripline of a single fanout
243 card was measured using the network analyzer to be 29.7 mm.

244 Measurements were made with anodes consisting of a continuous ground-
245 plane and the strip-line covered glass base of 1, 3, and 4 tiles, where each tile
246 anode is 229.1 mm-long. In addition, measurements were made with a 115
247 mm-long ‘half-tile’, and, in order to unfold the contribution of the fanout cards
248 themselves, with the zero-tile configuration. Figure 4 shows the zero-tile and
249 3-tile setups used in conjunction with the single tile (Figure 3) to measure

250 bandwidth, attenuation, and impedance as a function of anode strip length.
251 The connections between anodes are made by hand soldering small strips of
252 copper to the silver silk-screened strips on the glass.



Figure 5: The geometry of the coupling between the coaxial cable from the pulse generator to the anode strip before modification (Left) and after correction with copper tape (Right).

253 4.2. Launchers

254 The transition of the \vec{E} and \vec{B} fields between the geometries of the coaxial
255 cable, the SMA cable, and the planar transmission line results in reflections
256 and signal distortion. This can be handled by designing a transition region, or
257 ‘launcher’ to match the impedances. Rather than using a full wave simulator
258 to get a theoretical solution, we used an empirical method of tuning by hand
259 while watching the match with a network analyzer. We used adhesive-backed
260 copper tape [31] to construct geometries on the glass substrate. Monitoring the
261 work in the time domain on a network analyzer, one can identify the location of
262 impedance mismatches and make appropriate additions (more capacitance) or
263 subtractions (more inductance) of metal. After optimization a single launcher
264 shape was adequate for all the strips in the 30-strip tile, as expected.

265 The left-hand panel of Figure 5 shows the geometry of the coupling between
266 the coaxial cable from the pulse generator to the anode strip before modification,
267 and on the right, after correction.

268 *4.3. Measurements of Pulse Rise Times*

269 The anode responses to a step-function with a risetime of 200 psec introduced
270 into one end of a strip in a multi-strip anode were measured using the reference
271 fast edge of the calibration output from a Tektronix TDS6154C scope, as shown
272 in Figure 6. The 30-strip anode has better bandwidth performance than the
273 40-strip due to less coupling to neighboring strips. The length of the anode also
274 enters into performance, as the energy transfer to neighboring strips grows with
275 strip length.

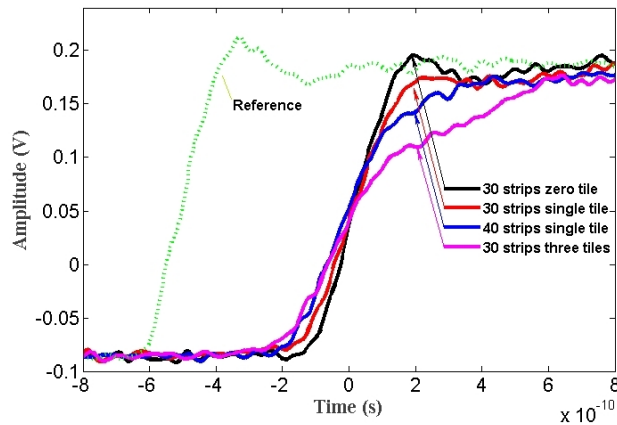


Figure 6: The anode responses in the time domain to a step-function introduced into one end of a strip in a multi-strip anode. The source of the reference pulse is the calibration output from a Tektronix TDS6154C oscilloscope, which has a risetime of 200 psec and an amplitude of 440 mV (peak-peak). The response curves in the figure were measured with the same oscilloscope.

276 *4.4. Measuring the Bandwidth, Attenuation, Velocity, and Impedance*

277 Measurements of analog bandwidth, attenuation, propagation velocity, cross-
278 talk, impedance, and RF matching were made with an Agilent HP8753E network
279 analyzer [32]. For each tile configuration, signals were introduced from one port
280 on one end of an anode strip via a fanout card, and measured at the far end via
281 a second fanout card. The power on both the near end and the far end were

282 recorded as a function of frequency. The signals on both ends of neighboring
 283 strips were also recorded. The results are given in Sections 5, 6, and 7 below.

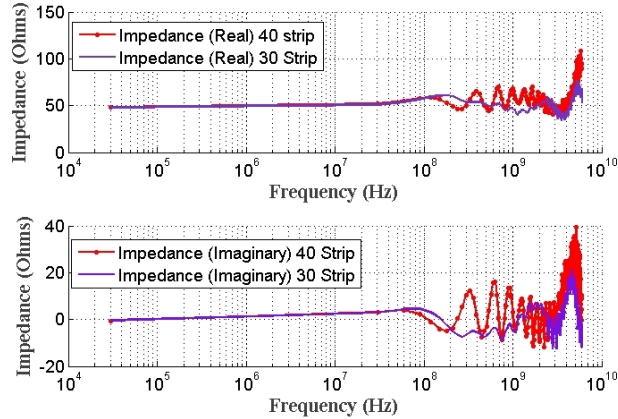


Figure 7: The measured real (top) and imaginary (bottom) impedance versus frequency for 40-strip and 30-strip silk-screened anodes on a single 229.1 mm-long glass tile base between two fanout cards. The targeted design impedance (top) was 50Ω s .

284 5. Impedance

285 The impedance of a single strip of width w separated from an infinite ground
 286 plane by a glass substrate of thickness h depends on the ratio of strip width to
 287 strip-ground plane separation, w/h , as described in Appendix A [33].

288 In the case of an array of multiple striplines, the impedance of the lines is
 289 more complicated, as the geometry of the field lines is affected by the adjacent
 290 strips. Consequently additional excitation (odd and even) modes exist, modify-
 291 ing the impedance of the single stripline mode [34, 35]. The impedance of the
 292 lines is thus not only a function of the w/h ratio but also of the width of the
 293 gap between the strips.

294 Figure 7 shows the measured real and imaginary parts of the impedance ver-
 295 sus frequency for 40-strip and 30-strip silk-screened anodes on a single 229.1 mm-

296 long glass tile base between the fanout cards. The targeted design impedance
 297 (real part) was 50Ω . The impedances are well-matched to the few-GHz band-
 298 width of the present MCP's. The imaginary part of the 'frugal' 30-strip anode
 299 stays relatively small up to the few-GHz region, well-matched to the bandwidth
 300 of the present LAPPD 220-mm-square 20-micron pore MCP's.

301 **6. Bandwidth**

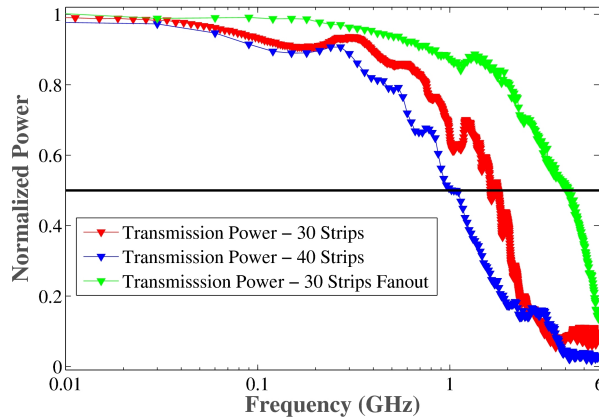


Figure 8: The normalized power (output power/input power) for a single 229.1 mm-tile plus fanout cards(288.5 mm) with 30 strips (red), 40 strips (blue), and the fanout PC cards alone('zero-tile', in green). See Figure 3. The black horizontal line represents the 3db loss level (50% loss in power).

302 In a stripline anode geometry, a wave travelling on one strip will also transfer
 303 energy to its neighbors due to inductive and capacitive coupling between the
 304 striplines [34, 35]. We have measured the bandwidth over a different length of
 305 striplines by connecting the 229.1 mm anode of the tile to a neighboring tile or
 306 tiles in series, as shown in Figure 4.

307 Figure 8 shows the measured ratio of output power to input power versus
 308 frequency for the three cases of a single 30-strip anode with fanout cards, a
 309 single 40-strip anode with fanout cards, and just the fanout cards alone ('zero-

310 tile'). The 30-strip tile has significantly improved analog bandwidth, as well
311 as providing the reduced channel count for the 6-channel PSEC-4 ASIC. No
312 correction has been made for the fanout cards, as they have significantly higher
313 bandwidth than the anodes.

314 Figure 9 shows the measured 3-dB loss point in frequency for different length
315 anodes. The points shown correspond to the effective length of the fanout card
316 pair alone (59.4 mm), a single tile with fanout cards (288.5 mm), and, in the
317 case of the 30-strip anode, three and four tiles with fanout cards (746.7 mm and
318 916 mm, respectively). The slope of the exponential fit of the bandwidth (GHz)
319 versus the log of the length in cm is -3.19, and the intercept is 6.42 GHz.

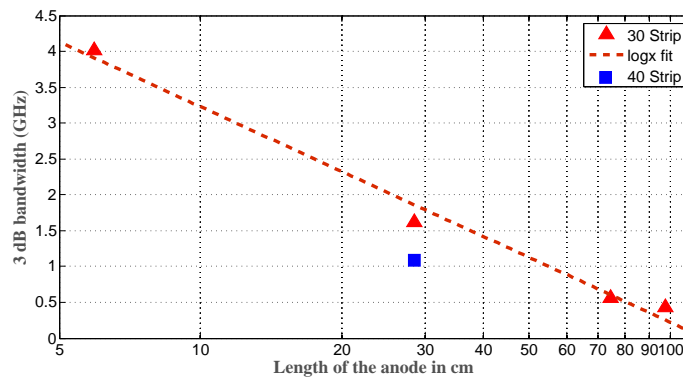


Figure 9: The bandwidth measured at 3db loss on the central strip for different length anodes between a pair of fanout cards. Anodes consisting of 3 and 4 tiles in series (746.7 mm and 916 mm, respectively), a single tile (288.5 mm), and only the 2 fanout PC cards connected to each other ('zero tiles'- 59.4 mm) on a log scale.

320 **7. Attenuation and Cross-talk**

321 The power in a pulse propagating down a strip diminishes with distance due
 322 to resistive attenuation in the materials of the strip and coupling to neighboring
 323 strips. Two adjacent striplines are both capacitively and inductively coupled.
 324 A wave travelling down the line induces a signal on its neighbor both in the
 325 forward and reverse direction. This cross-talk, which is the dominant source of
 326 loss at high frequencies, produces pulses both at the near and far end of the
 327 adjacent strips, as shown in Figure 10. The degree of acceptable energy loss
 328 and signal mixing from one strip to another is application-specific, and can be
 329 optimized by changing the strip spacing and impedance, or by using a material
 330 with an appropriate dielectric constant.

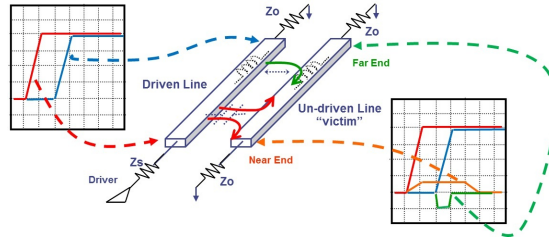


Figure 10: The mechanism of cross-talk. Two adjacent striplines are both capacitively and inductively coupled. The initial excitation of one line, the driven line, is from the charge cloud of the MCP stack. This results in two pulses travelling away from the initial excitation towards the ends of the driven line. Each of these two pulses induces a signal on its neighbor both in the forward and reverse direction (the dashed lines).

331 Figure 11 shows measurements of the normalized power measured in the
 332 driven strip (Strip 0) and neighboring strips. A signal is input on the central
 333 strip (shown in red) via the fanout card and is detected at the far end. The
 334 power is measured on the near and far ends of the strips. The left-hand plot
 335 shows the sum of the two ends for each strip. A single 30-strip tile is shown as
 336 triangles; measurements on an anode made of three 30-strip tiles in series (see
 337 Figure 4) are represented by squares. A single 40-strip tile is shown as circles.

338 The single 30-strip tile has the lowest cross-talk, as expected due to its wider
 339 spacing than the 40-strip tile and shorter length than the anode composed of
 340 three 30-strip tiles. The effect of cross-talk on pattern recognition will depend
 341 on the specific application (specifically occupancy and signal-to-noise), and the
 342 implementation of digitization and pattern-recognition algorithms.

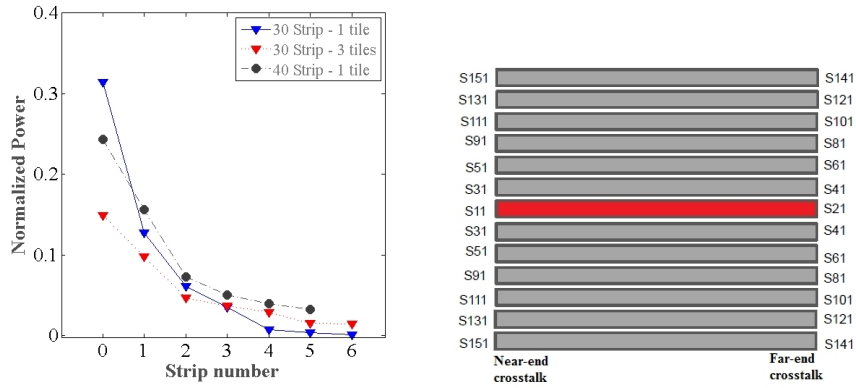


Figure 11: Comparison of total normalized power summed over all striplines for three different anode geometries: a single 30-strip tile (triangles), a single 40-strip tile (circles), and three 30-strip tiles in series. The right-hand panel shows the geometry of the test setup: A signal (S11) is input on the central strip (shown in red) and is detected at the far end (S21). The power is measured on the near and far ends of the neighboring strips.

343 8. Conclusions

344 Anodes for MCP-PMT's with analog bandwidths in the GHz region are pre-
 345 dicted to enable sub-psec time resolutions for applications that provide enough
 346 initial signal. We have measured the signal properties of a class of inexpen-
 347 sive anodes for use in large-area microchannel plate detectors and other current
 348 sources. The strip-line anodes are inexpensively constructed by silk-screening
 349 silver ink on widely-available borosilicate float glass. The unit 'tile' anode is
 350 229-mm long; the units can be daisy-chained in series to cover more area with

351 the same electronics channel count. The present LAPPD ‘frugal’ design uses 30
352 anode strips to cover the 220-mm wide anode.

353 We measure an analog bandwidth of 1.6 GHz on a single tile, and present
354 the bandwidth as a function of the number of tiles for anode strip lines up to
355 916 mm in length. Results on attenuation, cross-talk, impedance, and signal
356 velocity are also presented. We also describe the techniques and equipment used
357 in the measurements.

358 **9. Acknowledgments**

359 We thank our colleagues in the Large Area Psec Photodetector (LAPPD)
360 Collaboration for their contributions and support. Particular thanks are due
361 to F. Tang for his initial suggestion and work on parallel strip lines, M. Heintz
362 for critical technical support, G. Varner for RF advice, and R. Metz and M.
363 Zaskowski for machining and mechanical work. J. Gregar (ANL), P. Jaynes
364 (CatI Glass), and E. A. Axtell (Ferro Corporation) provided invaluable advice
365 and technical support.

366 The activities at Argonne National Laboratory were supported by the U.
367 S. Department of Energy, Office of Science, Office of Basic Energy Sciences
368 and Office of High Energy Physics under contract DE-AC02-06CH11357, and
369 at the University of Chicago by the National Science Foundation under grant
370 PHY-1066014.

372 **10. Appendix A: Single Strip Bandwidth and Impedance**

373 The dependence for the two cases of $w/h < 1$ and $w/h > 1$ are given in
 374 Equ. 1 [33].

if: $\frac{w}{h} \leq 1$:

$$\begin{aligned} \epsilon_{eff} &= \frac{\epsilon_r + 1}{2} + \frac{\epsilon_r - 1}{2} \left(\frac{1}{\sqrt{1 + 12\frac{h}{w}}} + 0.04 \left(1 - \frac{w}{h}\right)^2 \right) \\ Z_0 &= \frac{60}{\sqrt{\epsilon_{eff}}} \ln \left(8\frac{h}{w} + 0.25\frac{w}{h} \right) \end{aligned} \quad (1)$$

if: $\frac{w}{h} \geq 1$:

$$\begin{aligned} \epsilon_{eff} &= \frac{\epsilon_r + 1}{2} + \frac{\epsilon_r - 1}{2\sqrt{1 + 12\frac{h}{w}}} \\ Z_0 &= \frac{120\pi}{\sqrt{\epsilon_{eff}} \left(\frac{w}{h} + 1.393 + \frac{2}{3} \ln \left(\frac{w}{h} + 1.444 \right) \right)} \end{aligned}$$

375 **References**

- 376 [1] T. Credo (IMSA), H. Frisch, H. Sanders, R. Schroll, and F. Tang; *Picosec-*
377 *ond Time-of-Flight Measurement for Colliders Using Cherenkov Light*; Pro-
378 ceedings of the IEEE, Rome, Italy, Oct. 2004; Nuclear Science Symposium
379 Conference Record, 2004 IEEE, Volume: 1 Date: 16-22 Oct. 2004.
- 380 [2] J.-F. Genat, G. S. Varner, F. Tang, H. Frisch; *Signal Processing for Pico-*
381 *second Resolution Timing Measurements*, Nucl. Instr. Meth. A607, p387,
382 Oct. 2009; e-Print: arXiv:0810.5590
- 383 [3] J.L. Wiza, Micro-channel Plate Detectors. Nucl. Instr. Meth. 162, p567;
384 1979
- 385 [4] A.S. Tremsin and O.H.W. Siegmund, “Charge cloud asymmetry in detec-
386 tors with biased MCPs” Proceedings SPIE3, vol. 4497, San Diego, Califor-
387 nia (2001)
- 388 [5] K. Inami, N. Kishimoto, Y. Enari, M. Nagamine, and T. Ohshima; Nucl.
389 Instr. Meth. A560, p.303, 2006
- 390 [6] J. Milnes and J. Howorth (Photek Ltd.), “Advances in Time
391 Response Characteristics of Micro-channel Plate PMT Detectors”.
392 See http://www.photek.com/support/technical_papers.htm (website says:
393 ‘Ref. not yet available’).
- 394 [7] S. Ritt, in *The Factors that Limit Time Resolution in Photodetec-*
395 *tors*; Workshop, Univ. of Chicago, Chicago, IL; 28-29 April 2011. See
396 <http://psec.uchicago.edu/workshops/> Note that of the values needed of the
397 four parameters to achieve a time resolution of 100 fsec (the bottom row
398 of the table of extrapolations), we have achieved or exceeded three: sam-
399 pling rate, noise, and signal size. Only the analog bandwidth falls short at
400 present.
- 401 [8] M. Lampton, *Delay line anodes for microchannel plate spectrometers* Rev.
402 Sci. Instr. Vol. 58, 12, 2298, 1987;

- 403 [9] O.H.W. Siegmund, *Amplifying and position sensitive detectors*”, in “Methods
404 of vacuum ultraviolet physics”, Chapter III, 2nd edition; editors J.A.R.
405 Sampson and D. L. Ederer, Academic Press, 1998.
- 406 [10] O. Jagutzki et al., *Multiple Hit Readout of a Microchannel Plate Detector*
407 *With a Three-Layer Delay-Line Anode*, IEEE Trans. on Nucl. Sci. Vol. 49,
408 No.5, 2477 (2002)
- 409 [11] J.S. Lapington, J.R. Howorth, J.S. Milnes; *Demountable readout technologies for optical image intensifiers*, Nucl. Instr. Meth. A573, p243 (2007)
410
- 411 [12] The original LAPPD institutions include ANL, Arradance Inc., the
412 Univ. of Chicago, Fermilab, the Univ. of Hawaii, Muons,Inc, SLAC,
413 SSL/UCB, and Synkera Corporation. More detail can be found at
414 <http://psec.uchicago.edu/>.
- 415 [13] For a discussion of the factors that determine time and space resolution
416 in MCP-based detectors, see the talks at: *The Factors that Limit Time*
417 *Resolution in Photodetectors*; Workshop, Univ. of Chicago, Chicago, IL;
418 28-29 April 2011. See <http://psec.uchicago.edu/workshops/>
- 419 [14] The glass capillary substrates are produced by Incom Inc. Charlton Mass.
420 See <http://www.incomusa.com/>.
- 421 [15] S. M. George, *Atomic Layer Deposition: An Overview*; Chemical Reviews
422 2010, 110, (1), 111-131
- 423 [16] J. W. Elam, D. Routkevitch, and S. M. George, *Properties of ZnO/Al₂O₃*
424 *Alloy Films Grown Using Atomic Layer Deposition Techniques*; Journal of
425 the Electrochemical Society 2003, 150, (6), G339-G347.
- 426 [17] D. R. Beaulieu, D. Gorelikov, H. Klotzsch, P. de Rouffignac, K. Saadat-
427 mand, K. Stenton, N. Sullivan, and A. S. Tremsin, *Plastic microchannel*
428 *plates with nano-engineered films*; Nucl. Instr. Meth. A633, S59-S61 (2011).

- 429 [18] O.H.W. Siegmund, J.B. McPhate, S.R. Jelinsky, J.V. Vallerga, A.S. Trem-
430 sin, R. Hemphill, H.J. Frisch, R.G. Wagner, J. Elam, and A. Mane, *Devel-*
431 *opment of Large Area Photon Counting Detectors Optimized for Cherenkov*
432 *Light Imaging with High Temporal and sub-mm Spatial Resolution*; IEEE
433 Transactions, Submitted, (2011).
- 434 [19] *Large Area, Pico-second Resolution, Time of Flight Detectors*;
435 US Patent US 2007/0187596 A1; Aug 16, 2007; Inventors: H. J. Frisch, H.
436 Sanders, F. Tang, T. Credo
- 437 [20] J.W. Elam, J. A. Libera, M.J. Pellin, and P.C. Stair, “Spatially Controlled
438 Atomic Layer Deposition in Porous Materials”, Applied Physics Lett., 2007
439 **91** (24)
- 440 [21] There are additional effects that make the focusing not exact- see, for ex-
441 ample, A.S. Tremsin, J.V. Vallerga, O.H.W. Siegmund, *Image translational*
442 *shifts in microchannel plate detectors due to the presence of MCP channel*
443 *bias*, Nucl. Instr. Meth. A477 (2002), 262.
- 444 [22] The measured transverse resolution for the 229-mm 30-strip anode excited
445 by pulses from the microchannel plate detector is 0.5 mm, comparable to
446 the longitudinal resolution of approximately 0.4 mm; detailed studies of the
447 assembled micro-channel plate detector will be presented elsewhere [36]. We
448 note that in applications such as a collider detector the unique capability of
449 a system of MCP-PMT’s is for psec-level TOF. Much more precise spatial
450 measurements are provided by the central tracking systems, but with much
451 poorer timing.
- 452 [23] J.-F. Genat, *Development of a Sampling ASIC for Fast Detector Signals*,
453 Workshop on Fast Timing, Cracow Poland, Nov. 2010
- 454 [24] M. Wetstein, B. Adams, A. Elagin, R. Obaid, et al. (the LAPPD Collabo-
455 ration), in preparation.

- 456 [25] B. Joly, Optimisation de la résolution temporelle en tomographie par
457 émission de positons dédiée au contrôle de dose en hadronthérapie;
458 Ph.D Thesis, Université Clermont Ferrand II- Blaise Pascal, Feb. 2010.
459 <http://tel.archives-ouvertes.fr/docs/00/50/51/29/PDF/BJoly.pdf>
- 460 [26] http://psec.uchicago.edu/glass/borofloat_33_e.pdf#page=28; The dielec-
461 tric constant is 4.6 and the loss tangent is 37×10^{-4} , both measured at
462 25C and 1 MHz.
- 463 [27] Ferro Corp., 251 Wylie Ave., Washington PA 15301
- 464 [28] Cat-I Glass, P.O. Box 208, S. Elgin, IL 60177
- 465 [29] E. Oberla, *A 4-Channel Fast Waveform Sampling ASIC in 130 nm CMOS*,
466 TIPP 2011, Chicago, IL., July 2011, Proceedings to be published in Physics
467 Procedia (Elsevier), 2012
- 468 [30] E. Oberla, *A Fast Waveform-Digitizing ASIC-based DAQ for a Position*
469 *& Time Sensing Large-Area Photo-Detector System*; Photodet2012, LAL
470 Orsay, France; June, 2012
- 471 [31] The adding or subtracting of a few-millimeter triangle of copper measurably
472 changes the capacitance and inductance at an interface, and is easily seen
473 with the network analyzer.
- 474 [32] Agilent Model HP8753E (6 GHz bandwidth) with Option 010 (time domain
475 option).
- 476 [33] I. J. Bahl and D. K. Trivedi, "A Designer's Guide to Microstrip Line",
477 Microwaves, May 1977, pp. 174-182.
- 478 [34] R. Harrington; Time Harmonic Electromagnetic Fields; IEEE Press, 1961
- 479 [35] R. Brown; Lines, Waves, and Antennas; John Wiley New York
- 480 [36] M. Wetstein, B. Adams, A. Elagin, J. Elam, H. Frisch, Z. Insepov, V.
481 Ivanov, S. Jokela, A. Mane, R. Obaid, I. Veryovkin, A. Vostrikov, R. Wag-
482 ner Alexander Zinovev et al., to be submitted to Nucl. Instr. Meth.